BURNT AREA DETECTION USING MEDIUM RESOLUTION SENTINEL 2 AND LANDSAT 8 SATELLITES

D. Ongeri[a]*and B. K. Kenduiywo[a,b]

[a]Department of Geomatic Engineering and Geospatial Information Systems,
Jomo Kenyatta University of Agriculture and Technology, Nairobi, Kenya - derickongeri@gmail.com, bkenduiywo@jkuat.ac.ke
[b]Environmental Science and Policy, University of California, Davis, USA - bkenduiywo@ucdavis.edu

Commission II, WG 10

KEY WORDS: Burnt Area, forest fire, Sentinel 2, Landsat 8

ABSTRACT:

Forest fire is one of the most serious environmental problems in Kenya that influences human activities, climate change and biodiversity. The main goal of this study is to apply medium resolution sensors (Landsat 8 OLI and Sentinel 2 MSI) to produce burnt area severity maps that will include small fires (<100 ha) in order to improve burnt area detection and mapping in Kenya. Normalized burnt area indices were generated for specified pre- and post-fire periods. The difference between pre- and post-fire Normalized Burnt Ration (NBR) was used to compute δNBR index depicting forest disturbance by fire events. Thresholded classes were derived from the computed δNBR indices to obtain burnt severity maps. The spatial and temporal agreements of the Burnt area detection dates were validated by comparing against the MODIS MCD641 500 m products and MODIS Fire Information for Resource Management System (FIRMS) 1 km daily product hot-spot acquisition dates. This approach was implemented on Google Earth Engine (GEE) platform with a simple user interface that allows users to auto-generate burnt area maps and statistics. The operational GEE application developed can be used to obtain burnt area severity maps and statistics that allow for initial accurate approximation of fire damage.

1. INTRODUCTION

Fire is a natural disturbance that profoundly influences people, climate and ecosystems to promote biodiversity (Kelly and Brotons, 2017). However, in the last centuries, human induced fires and suppression efforts have altered the natural fire regimes causing a negative effect on forest cover, resilience and biodiversity (Chuvieco et al., 2019; Lewis et al., 2015). In addition, a significant amount of aerosols and carbon emissions are caused by biomass burning critically affecting the atmospheric chemical composition (Knorr et al., 2016). Moreover, fires that occur in densely populated areas affect air quality and are linked with health impacts to infants, people with respiratory complications and individuals with heart problems (Reid et al., 2016). For instance in Kenya, forest fires occurring in Gathiuru forest have caused air pollution, visual problems and difficulties in breathing for the communities living around the forest and kilometers away as the smoke is carried by wind (Nyongesa and Vacik, 2018). Generally, as Viedma et al. (2017) puts it, Land Use-Land Cover (LULC) changes by human influence has led to more hazardous landscapes, with consequent increase in fires.

Most of the reported and documented forest fire occurrences in Kenya are small fires (<100 ha) that turn into large fires. The fires are mainly caused by human influence as a source of ignition with most of the reported actions being arson, honey gathering, charcoal burning and agricultural practices. High productive forests in Kenya, including both indigenous and plantation forests are located in relatively high fire prone areas. The fires continue to be one of the biggest hazard threats in these areas (Downing et al., 2017). On 23 February 2019 a fire believed to have been started by illegal marijuana farmers (as reported by local media) consumed up to 16,991 ha of moorland in Mount Kenya as estimated by Copernicus Emergency Management Service.

*Corresponding author.

Efforts have been made by the forest fire protection unit that is part of the Kenya Forest Service (KFS) to protect the fire prone forest areas from wild fires (Nyongesa and Vacik, 2018). Fire detection and monitoring is done by ground patrols and fixed stations (fire towers). During fire regimes the forest fire protection unit prepares a comprehensive report detailing the location, the area affected, cost of suppression and actual damage to the forest is compiled. Remotely sensed burnt area products from the KFS fire detection and monitoring unit are derived from coarse resolution satellite imagery obtained from MODIS 500 m sensors. However, the use of global burnt area products derived from coarse spatial resolution sensors such as MERIS (300 m), MODIS (250 m – 500 m) and AVHRR (1000 m), small fire detection and burnt area estimation becomes a challenge as noted by Padilla et al. (2015). Although less catastrophic than large fire regimes, small fires still play a significant role in carbon emissions and land use transformation (Roteta et al., 2019; Hutto et al., 2016; Lewis et al., 2015). The development of most of the global burnt area products was initially to fulfill the need for climate modelling as fire is considered an essential climate variable (Chuvieco et al., 2019), but their use for local and regional fire regimes was unprecedented. Fire severity and extent of damage to vegetation by fires can not also be measured accurately using coarse resolution sensors (Downing et al., 2017). This has given rise to an increasing demand for high accuracy and systematic delivery of burnt area products (Mouillot et al., 2014).

The need for improved estimation of burnt areas and fire severity has only been partially met (Huang et al., 2016) globally and in Kenya. To solve the problem of under-estimation of burnt areas and improve the knowledge of location and occurrence of wild fires, remote sensing techniques using high and medium resolution imagery have been applied (Roteta et al., 2019). The disturbances on vegetation due to fire events has been studied using vegetation indices computed from Visible and Near Infra-Red (NIR) portions. For example, Normalized Difference Vegetation Index (NDVI) (Verhegghen et al., 2016; Navarro et al., 2017; En-

gelbrecht et al., 2017), NDVI red-edge 2 narrow (Navarro et al., 2017), and burnt area index (Roteta et al., 2019). However, the red band in the visible portion of the electromagnetic spectrum is affected by atmospheric haze and is susceptible to scattering (Langner et al., 2018; Verhegghen et al., 2016).

To overcome the limitations of using optical sensors, other studies have used microwave images to compliment the use of vegetative indices used for burnt area detection from optical sensors (Verhegghen et al., 2016). Nonetheless, fires result in ambiguous effects in radar images depending on the radar wavelength, polarization, and meteorological conditions at image acquisition (Lohberger et al., 2018; Verhegghen et al., 2016; Chuvieco et al., 2019).

This study looks into the lack of a harmonized burnt area detection and mapping approach using medium spatial resolution optical imagery. We adopt Landsat 8 and Sentinel 2 medium resolution sensors to solve the challenge of under-estimation of burnt areas and to improve the knowledge of spatial and temporal occurrence of wild fires in Kenya. A Google earth engine application that uses the medium resolution images to generate burnt area products, that includes small fires (<100 ha) to show their potential for improving burnt area detection and mapping in Kenya, was developed.

2. MATERIALS AND METHODS

2.1 Study area and data

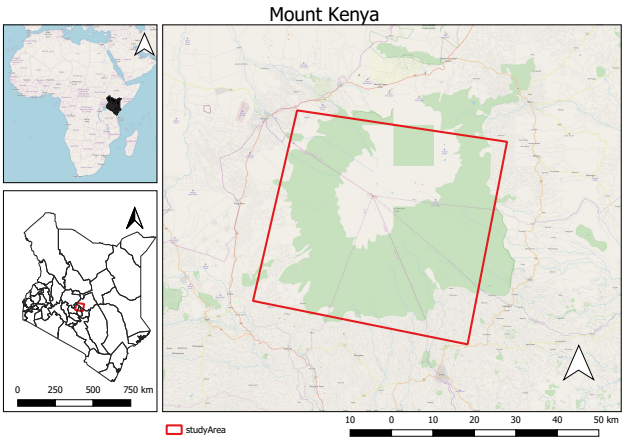

Figure 1. Study Area

We chose to conduct the study in Mount Kenya (Figure 1) because fire has been a major hazard affecting the forest area (Nyongesa and Vacik, 2018). The slopes of the mountain are covered by different types of vegetation and forest. It is surrounded by 715 km^2 of national park that is protected by the Kenya wildlife service (KWS). The forest is located in the counties of Meru, Embu, Laikipia, Kirinyaga, Nyeri and Tharaka Nithi. The forest areas of the park are under administration of the KFS.

This study used Moderate Resolution Imaging Spectroradiometer (MODIS) MCD64A1 product series, Landsat 8 and Sentinel 2 satellite images available on Google Earth Engine (GEE) API. The data properties are summarized in Table 1. We also used fire reference data that was recorded by the KFS and corresponding forest boundaries.

2.2 Burnt area detection

The overall methodological approach that was used to implement this study is summarized in Figure 2.

Table 1. Data and data Sources

Data	Provider	Spatial-resolution	Temporal resolution
Landsat 8	USGS	30 m	16 days
Sentinel 2	ESA	10 m	5 days
MODIS	NASA	500 m	Monthly

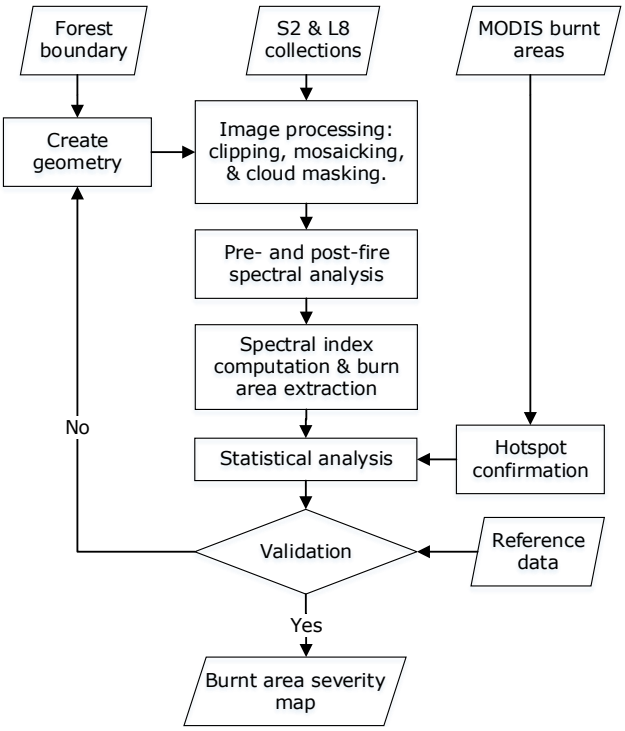

Figure 2. Methodological framework adopted to detect small extent fires using GEE.

2.2.1 Creation of image bounds: Since the full extents and perimeter of the fire were unknown the boundary of the study area was digitized interactively on GEE using gazetted legal forest boundaries as guide to capture the whole extents of fire incidences. The resulting polygons formed the clipping bounds for the pre and post-fire images.

2.2.2 Image selection and pre-processing: Sentinel-2 MSI Level-2A and Landsat 8 surface reflectance Tire 1 were selected for the study. To obtain a collection of images, both pre- and post-fire date ranges were used. The periods as opposed to single dates ensured the availability of images. A cloud filter was applied to ensure that the best quality images are selected for analysis. All selected images overlapping the study area were then mosaicked and clipped to the bounds of the study area. A cloud and snow mask was applied to the images using the pixel quality bands in respective Landsat 8 and Sentinel 2 images. This was done in order to correct for atmospheric effects and to obtain cloud free images.

2.2.3 Spectral analysis: From the cloud free images, 52 randomly selected points were classified as burnt or unburnt using the MODIS burnt area monthly global 500 m product from MCD64A1 series. Spectral charts were then generated from the randomly selected points to determine the spectral behavior of the burnt and unburnt pixels. Spectral bands most sensitive to fire in both Sentinel 2 and Landsat 8 were then used to compute burnt area indices and the results compared. The best performing index was

then selected for burnt area detection and severity mapping.

2.2.4 Burnt Area Spectral Indices **Normalized Burnt Ratio (NBR)** index in Equation (1) was computed for both pre- and post-fire images. This index was computed using the NIR (0.85–0.88 μm), corresponding to band 5 of Landsat 8 and band 8 of Sentinel 2, and SWIR window (2.11–2.29 μm) that corresponds to band 7 of Landsat 8 and band 12 of Sentinel 2. Eq. (1) shows how the NBR index was computed.

$$NBR = \frac{\rho_{NIR} - \rho_{SIR_2}}{\rho_{NIR} + \rho_{SIR_2}} \quad (1)$$

To get the disturbances due to fire from the pre- and post-fire images δNBR values were computed from the difference of pre- and post-fire NBR values as shown in Equation (2). The δNBR values were scaled by 10^3.

$$\delta\text{NBR} = \text{NBR}_{\text{pre-fire}} - \text{NBR}_{\text{post-fire}} \quad (2)$$

Mid-Infrared Burn Index (MIRBI) was computed from short and long SWIR bands of Sentinel 2 sensor. The shortwave infrared short (ρ_{SWIRS}) which corresponds to band 11 of Sentinel 2 and band 6 of Landsat 8 while the shortwave infrared long (ρ_{SWIRL}) which corresponds to band 12 of Sentinel 2 and band 7 of Landsat 8 were used as in Equation (3) and Equation (4).

$$\text{MIRBI} = 10 \times \rho_{\text{SWIRL}} - 9.8 \times \rho_{\text{SWIRS}} + 2 \quad (3)$$

Normalized Burnt Ratio 2 (NBR2)
The NBR2 was computed using Equation (4) from the same spectral bands as those used to compute the MIRBI in Equation (3).

$$\text{NBR2} = \frac{\rho_{\text{SWIRS}} - \rho_{\text{SWIRL}}}{\rho_{\text{SWIRS}} + \rho_{\text{SWIRL}}} \quad (4)$$

2.2.5 Burnt Area Severity: To determine the burnt area severity, δNBR values were classified using thresholds as recommended by Downing et al. (2017). Additional classes to include enhanced regrowth for post fire analysis were added as recommended by the United States Geological Survey (USGS). The Table 2 illustrates the burnt severity classes and the thresholds chosen.

Table 2. Burn severity categories.

Burn Severity	**δNBR range(unscaled)**	**δNBR range (scaled by10^3)**
Enhanced regrowth, high (postfire)	-0.500 to -0.250	-500 to -250
Enhanced regrowth, low (postfire)	-0.251 to -0.100	-250 to -100
Unburnt	-0.101 to 0.100	-100 to 100
Low Severity	0.101 to 0.269	101 to 269
Moderate-Low Severity	0.270 to 0.439	270 to 439
Moderate-High Severity	0.440 to 659	440 to 659
High Severity Burn	0.660 to 1.300	660 to 1300

2.2.6 Burnt area statistics: Burnt area statistics were then computed to determine burnt area in each of the severity classes. This was done by counting the number of pixels per class and subsequently computing the percentage area and the area in hectares. A mask of the entire burnt area was first extracted from the classified and the total number of pixels in the image counted to compute the total burnt areas in hectares. Similarly, pixel counts from single masks of each of the severity classes were used to compute the burnt area for each class and subsequently compute the burnt area for each of the classes as a percentage of the total burnt area. The computed areas were then compared to the reported areas by the KFS forest fire protection unit.

3. RESULTS

Results from pre- and post-fire spectral analysis are presented in Figure 3. The y-axis represent reflectance values from sentinel 2 MSI level-2 images multiplied by 10000. Before the fire event, there was high spectral reflectance in the NIR band (0.85–0.88 μm) corresponding to band 5 of Landsat 8 and band 8 of Sentinel 2. After the fire, the chart illustrates a drop in NIR spectral reflectance. This is because NIR is sensitive to chlorophyll content in vegetation hence it drops if vegetation is destroyed (Downing et al., 2017). The low spectral reflectance values of unburnt areas in the SWIR window (2.11–2.29 μm) that corresponds to band 7 of Landsat 8 and band 12 of Sentinel 2, increased after the fire. This was used as a selection criteria for the spectral indices to be used for detection of burnt areas.

Figure 4 illustrates detected areas based on indices computed using selected bands from Sentinel 2 and Landsat 8. The δNBR (Figure 4b) extracted severely burnt areas including its surroundings well when visually compared to the reference image in (Figure 4a). The modified NBR (Figure 4c) captured the severely burnt areas and the actively burning areas leaving out the moderate and low severity areas where the vegetation was disturbed as depicted by the reference data in (Figure 4a). This yeilded a consevertive estimate of the burnt area. MIRBI (Figure 4a) detected a larger burnt area than the modified NBR but could not capture moderate and low severity areas as shown in (Figure 4a). The also yielded a conservative estimate of the burnt area.

Figure 5a and Figure 5b show burnt area severity classes for Landsat 8 and Sentinel 2 respectively obtained from classifying δNBR values. Both figures show a large proportion of the burnt area is of moderate to high severity with a few pixels of low severity. Pre- and post-fire Sentinel 2 (Figure 5a) images captured the full extent of the fire while the Landsat 8 (Figure 5b) images did not capture the full extend of the fire due to the cloud mask applied to the images hence the no data values present in (Figure 5b). Statistics obtained for each of the burnt area severity classes indicates that 16,080 ha are moderate to highly severe areas as can be noted from (Table 3).

Table 3. Burn severity statistics.

Burn Severity	**Area in ha.**
Enhanced regrowth, high (postfire)	N/a
Enhanced regrowth, low (postfire)	N/a
Unburnt	11648.34
Low Severity	431.06
Moderate-Low Severity	4378.24
Moderate-High Severity	7691.76
High Severity Burn	4010.67

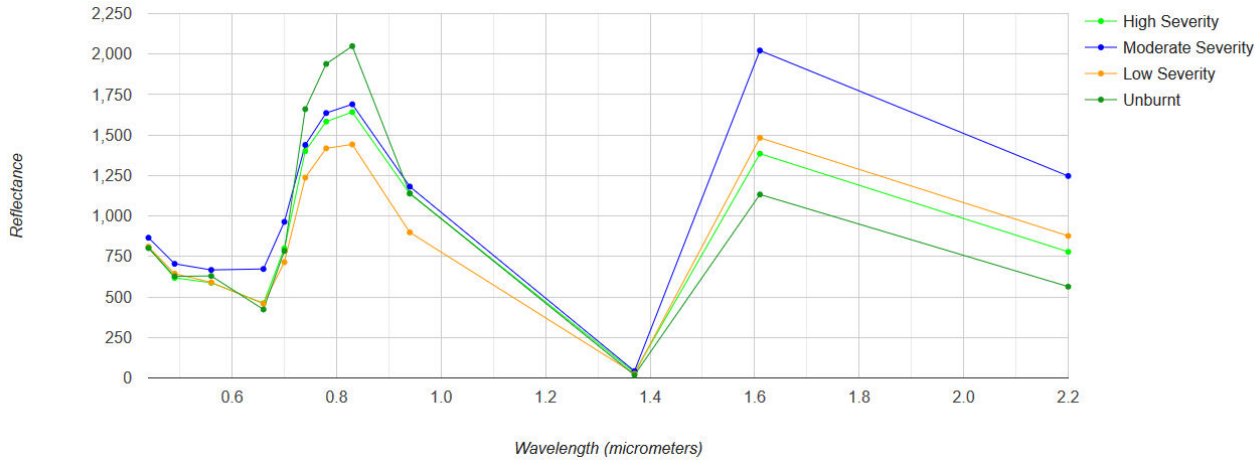

(a) Pre-fire spectral reflectance

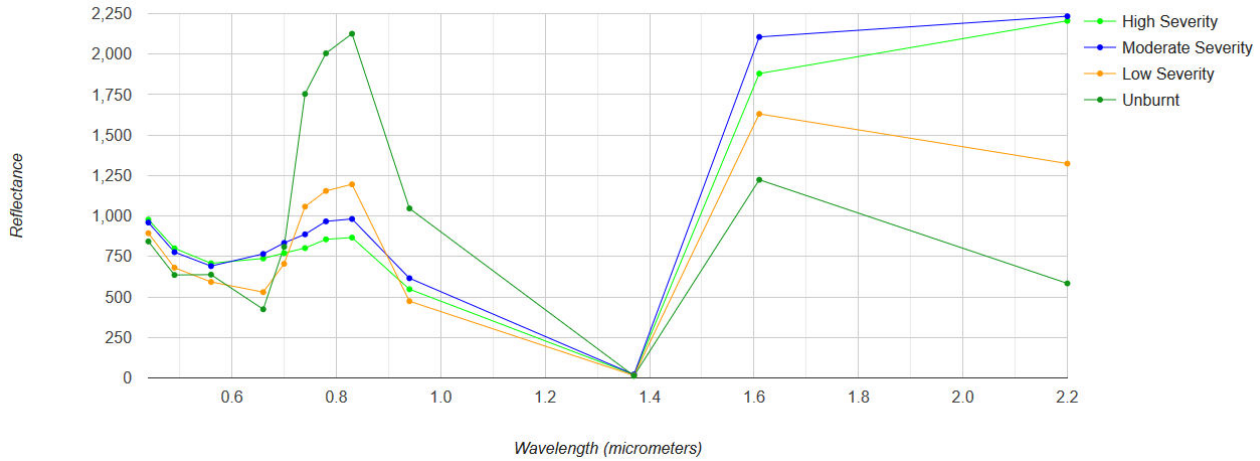

(b) Post-fire spectral reflectances

Figure 3. Spectral reflectance of pre- and post-fire images.

Validation was carried out with the current MODIS burnt area product in MCD64A1 series (Giglio et al., 2016) a product used by most atmospheric carbon modelers (Roteta et al., 2019). The spatial and temporal agreements of the Burnt area detection dates were validated by comparing against the MCD641 (500m) and the MODIS Fire Information for Resource Management System 1km daily product (FIRMS) hotspot acquisition date (Figures 6 and 7).

Detected burnt areas were also validated by comparing it against the reported KFS data and the extents reported by the Copernicus Emergency Management Service for the Mt. Kenya forest fire case study. The burnt area mapping tool was also tested for the Aberdare January 2017 fire incident and the Mt. Kenya (Meru) fire incident that occurred on 2–5 January 2018. The results are as summarized in Table 4.

Table 4. Comparison of detected burnt areas versus the ones reported in hectares (ha).

Forest Block	Date	Detected	Reported	Omission error
Aberdare	13–18 Jan 2017	6275.27	6594.37	4.84 %
Meru	2–5 Feb 2018	279	300	7 %
Mt. Kenya	23 Feb–02 Mar 2019	16080.	16991	5.36 %

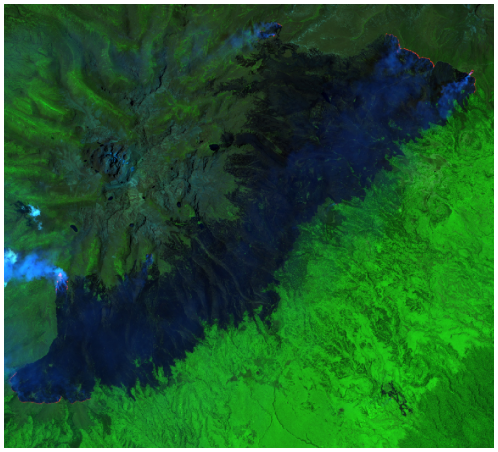

(a) Fire perimeter shown by sentinel 2 false-color composite.

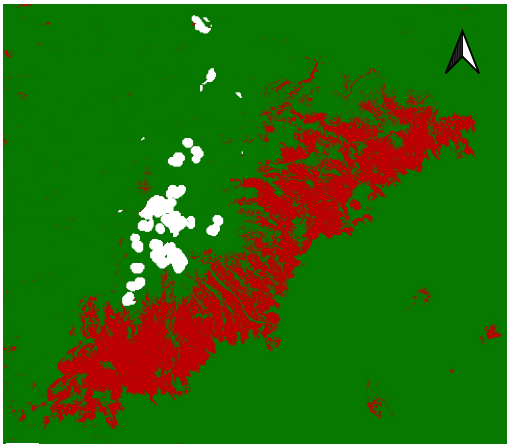

(b) Burnt area detected by δNBR.

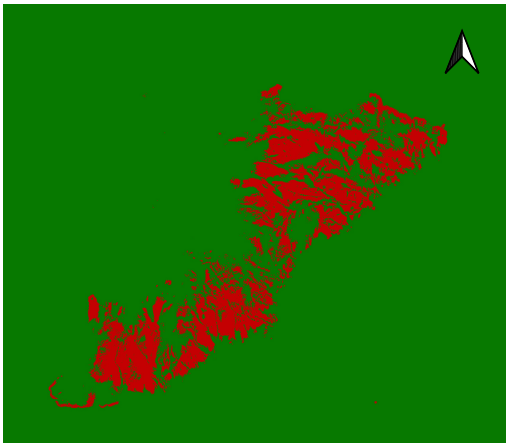

(c) Burnt areas in modified NBR.

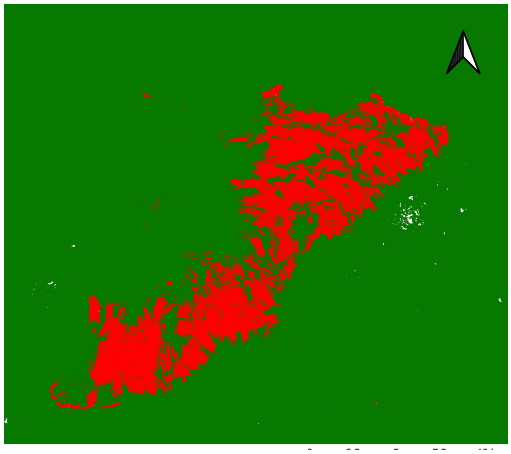

(d) MIRBI fire areas.

Figure 4. Burnt area (red colour) detected using different spectral indices.

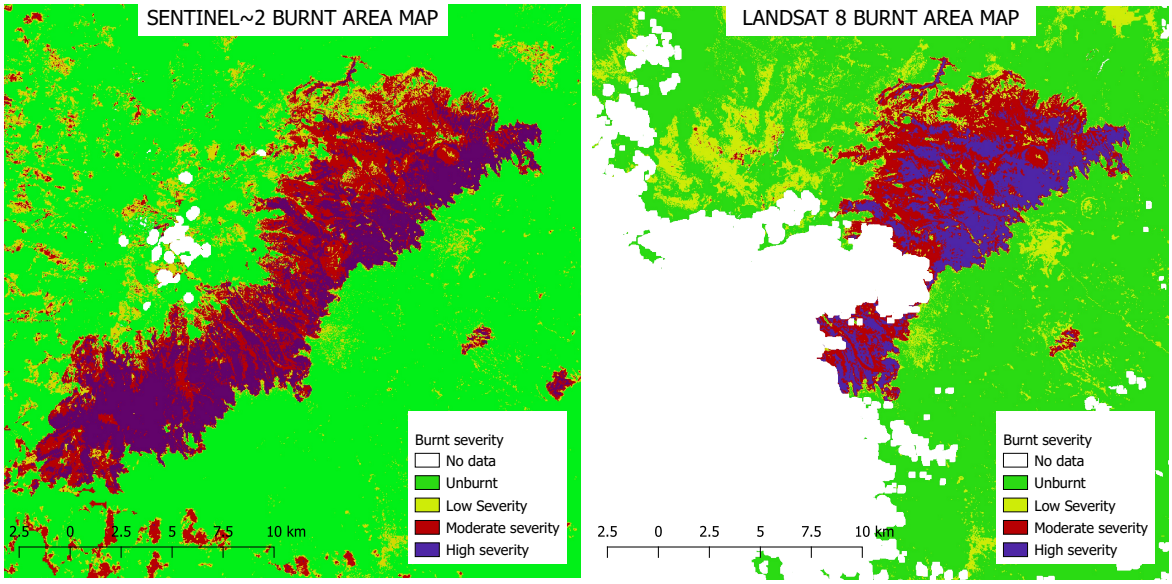

(a) Sentinel 2.

(b) Landsat 8.

Figure 5. Mt. Kenya burnt area severity

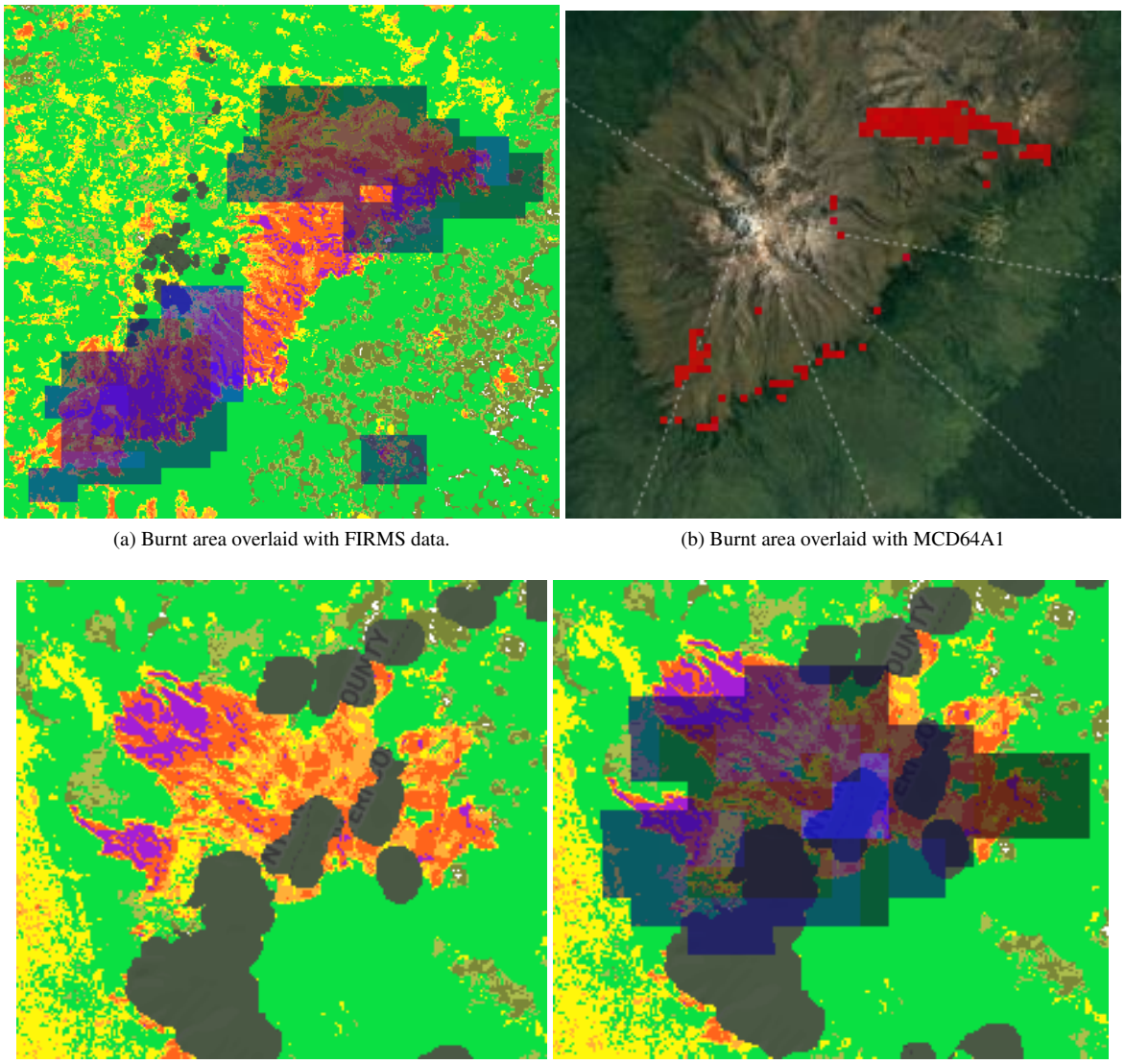

(a) Burnt area overlaid with FIRMS data.

(b) Burnt area overlaid with MCD64A1

(c) Aberdare Forest fire 13-18 Feb 2017 data

(d) Burnt area overlaid with FIRMS

Figure 6. Detected burnt areas in Aberdare overlaid with different datasets.

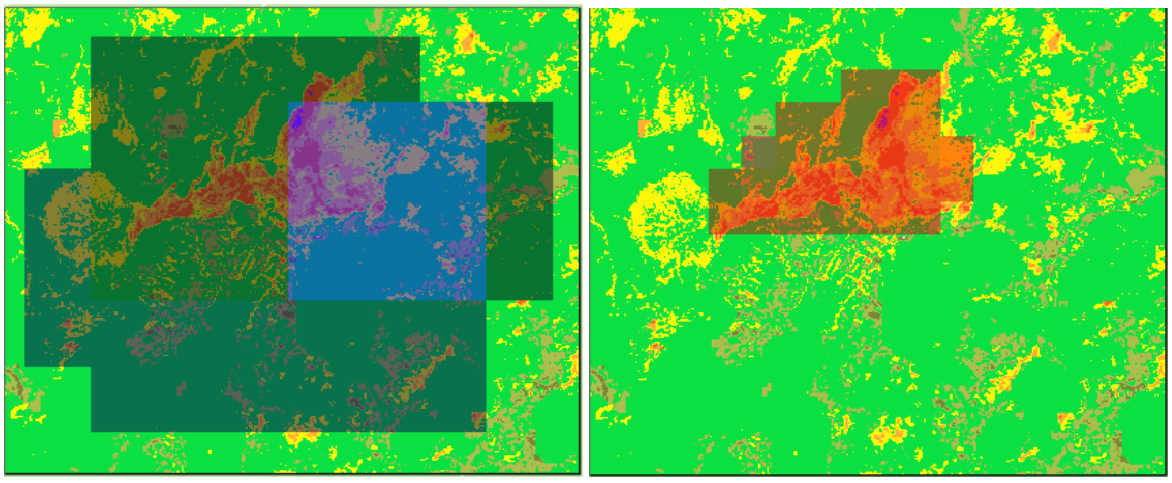

(a) Mt.Kenya Forest fire 03-05 Feb 2018 overlaid with FIRMS data.

(b) Burnt area overlaid with MCD64A1

Figure 7. Detected burnt areas in Mt. Kenya overlaid with different datasets.

4. DISCUSSION

The aim of our study was to detect small fires, that have otherwise been underestimated, using medium resolution Sentinel 2 and Landsat 8 images. Findings from our study indicate that these fires can be detected to an accuracy of an average omission error of 5.73%. The NIR and SWIR were the most useful in detecting changes associated with fire incidences. NIR is sensitive to chlorophyll content of plants hence it subsequently declined after a fire event. In contrast, healthy vegetation depicts low reflectance in SWIR band (Downing et al., 2017). Recently burnt areas demonstrate low reflectance in the NIR and high reflectance in the SWIR, i.e. the difference between the spectral responses of healthy vegetation and burnt areas reach their peak in the NIR and the SWIR regions of the spectrum as can be seen in Figure 3.

The MIRBI and the NBR2 indices used the shortwave infrared short (ρ_{SWIRS}) which corresponds to band 11 of Sentinel 2 and band 6 of Landsat 8 while the shortwave infrared long (ρ_{SWIRL}) which corresponds to band 12 of Sentinel 2 and band 7 of Landsat 8 (Roteta et al., 2019). While these can be used for burnt area detection, damage to vegetation could not be obtained hence the consideration of δNBR for both burnt area detection and burn severity mapping (Downing et al. (2017)) as shown in Table 2. In principle, the δNBR computed from the temporal analysis of pre- and post-fire images illustrates disturbances of vegetation by fire (Figure 5a). This makes tracking the recuperation of vegetation from fire possible; later dates for post-fire can be selected and the severity analyzed.

5. CONCLUSION AND OUTLOOK

This study developed a GEE application to detect burnt areas and determine burn severity from Landsat 8 OLI and Sentinel 2 MSI data. The tool was used for the approximation of burnt areas in other fire regimes in Aberdere Forest and Mount Kenya (Meru). The burn severity maps allows for accurate initial approximation of fire damage. Accurate burn severity maps not only quantify the damage to vegetation and hence loss in biodiversity, but can also aid in developing emergency rehabilitation and forest recovery plans.

ACKNOWLEDGEMENTS

We thank KFS for provision of fire reports data partly used in this study to validate predicted burnt areas.

References

Chuvieco, E., Mouillot, F., van der Werf, G. R., San Miguel, J., Tanase, M., Koutsias, N., García, M., Yebra, M., Padilla, M., Gitas, I., Heil, A., Hawbaker, T. J. and Giglio, L., 2019. Historical background and current developments for mapping burned area from satellite Earth observation. Remote Sensing of Environment 225, pp. 45–64.

Downing, T. A., Imo, M. and Kimanzi, J., 2017. Fire occurrence on Mount Kenya and patterns of burning. GeoResJ 13, pp. 17–26.

Engelbrecht, J., Theron, A., Vhengani, L. and Kemp, J., 2017. A Simple Normalized Difference Approach to Burnt Area Mapping Using Multi-Polarisation C-Band SAR. Remote Sensing.

Giglio, L., Schroeder, W. and Justice, C. O., 2016. The collection 6 MODIS active fire detection algorithm and fire products. Remote Sensing of Environment 178, pp. 31–41.

Huang, H., Roy, D. P., Boschetti, L., Zhang, H. K., Yan, L., Kumar, S. S., Gomez-Dans, J. and Li, J., 2016. Separability analysis of sentinel-2a multi-spectral instrument (msi) data for burned area discrimination. Remote Sensing.

Hutto, R. L., Keane, R. E., Sherriff, R. L., Rota, C. T., Eby, L. A. and Saab, V. A., 2016. Toward a more ecologically informed view of severe forest fires. Ecosphere 7(2), pp. e01255.

Kelly, L. T. and Brotons, L., 2017. Using fire to promote biodiversity. Science 355(6331), pp. 1264–1265.

Knorr, W., Jiang, L. and Arneth, A., 2016. Climate, CO_2 and human population impacts on global wildfire emissions. Biogeosciences 13(1), pp. 267–282.

Langner, A., Miettinen, J., Kukkonen, M., Vancutsem, C., Simonetti, D., Vieilledent, G., Verhegghen, A., Gallego, J. and Stibig, H., 2018. Towards operational monitoring of forest canopy disturbance in evergreen rain forests: A test case in continental southeast asia. Remote Sensing 10(4), pp. 1–21.

Lewis, S. L., Edwards, D. P. and Galbraith, D., 2015. Increasing human dominance of tropical forests. Science 349(6250), pp. 827–832.

Lohberger, S., Stängel, M., Atwood, E. C. and Siegert, F., 2018. Spatial evaluation of indonesia's 2015 fire-affected area and estimated carbon emissions using sentinel-1. Global Change Biology 24(2), pp. 644–654.

Mouillot, F., Schultz, M. G., Yue, C., Cadule, P., Tansey, K., Ciais, P. and Chuvieco, E., 2014. Ten years of global burned area products from spaceborne remote sensing — A review : Analysis of user needs and recommendations for future developments. International Journal of Applied Earth Observations and Geoinformation 26, pp. 64–79.

Navarro, G., Caballero, I., Silva, G., Parra, P., Vázquez, A. and Caldeira, R., 2017. Evaluation of forest fire on Madeira Island using Sentinel-2A MSI imagery. International Journal of Applied Earth Observations and Geoinformation 58, pp. 97–106.

Nyongesa, K. W. and Vacik, H., 2018. Fire Management in Mount Kenya: A Case Study of Gathiuru Forest Station. Forests.

Padilla, M., Stehman, S. V., Ramo, R., Corti, D., Hantson, S., Oliva, P., Alonso-Canas, I., Bradley, A. V., Tansey, K., Mota, B., Pereira, J. M. and Chuvieco, E., 2015. Comparing the accuracies of remote sensing global burned area products using stratified random sampling and estimation. Remote Sensing of Environment 160, pp. 114–121.

Reid, C. E., Brauer, M., Johnston, F. H., Jerrett, M., Balmes, J. R. and Elliott, C. T., 2016. Critical Review of Health Impacts of Wildfire Smoke Exposure. 1334(9), pp. 1334–1343.

Roteta, E., Bastarrika, A., Padilla, M., Storm, T. and Chuvieco, E., 2019. Development of a Sentinel-2 burned area algorithm: Generation of a small fire database for sub-Saharan Africa. Remote Sensing of Environment 222, pp. 1–17.

Verhegghen, A., Eva, H., Ceccherini, G., Achard, F., Gond, V., Gourlet-Fleury, S. and Cerutti, P. O., 2016. The Potential of Sentinel Satellites for Burnt Area Mapping and Monitoring in the Congo Basin Forests. Remote Sensing 8(12), pp. 1–22.

Viedma, O., Moreno, J. M., Güngöroglu, C., Cosgun, U. and Kavgacı, A., 2017. Recent land-use and land-cover changes and its driving factors in a fire-prone area of southwestern Turkey. Journal of Environmental Management 197, pp. 719–731.